



CHORUS

This is the accepted manuscript made available via CHORUS. The article has been published as:

α - β transformation and disorder in β -cristobalite silica

Fenglin Yuan and Liping Huang

Phys. Rev. B **85**, 134114 — Published 30 April 2012

DOI: [10.1103/PhysRevB.85.134114](https://doi.org/10.1103/PhysRevB.85.134114)

Nature of α - β transformation and disorder in β -cristobalite silica

Fenglin Yuan and Liping Huang¹⁾

*Department of Materials Science and Engineering, Rensselaer Polytechnic Institute, Troy, NY
12180, USA*

(Received

Disorder in β -cristobalite is shown to arise from the conformational changes between alpha- and beta-rings (energy barriers of 10-30 meV/SiO₂). Alpha-rings, remnants from the α - β transformation, constitute α -cristobalite. Beta-rings are local structures of a new β' -cristobalite of symmetry $\bar{I}4_2d$, confirmed herein by both molecular dynamics simulations and first-principles calculations. The ring conformation in β -cristobalite features a short correlation time (<50 fs) and short correlation length (<1 nm), giving the underlying topology framework the ability to support the dynamic disorder.

PACS numbers: 61.50.Ks, 61.66.Fn, 61.50.Ah

¹⁾ Electronic mail: huangL5@rpi.edu

I. INTRODUCTION

β -cristobalite, a high temperature and low-pressure polymorph of SiO_2 , is a technological important material, as there is a growing list of β -cristobalite-related phases (~ 100 to our knowledge) being discovered and a concerted effort is being made to explore them as engineering ceramics with high thermal shock resistance¹⁻⁴. On the other hand, β -cristobalite is often employed as a theoretical model to understand the structure of amorphous SiO_2 , which is essential to the performance of gate oxides at the Si/SiO_2 interfaces for microelectronic devices⁵ and of many glass forming systems⁶. However, despite a long history of experimental and theoretical investigations, the structure of high temperature β -cristobalite silica remains unsettled. Early experiments indicated a cubic structure of $\text{Fd}\bar{3}\text{m}$ symmetry⁷ for β -cristobalite (“ideal β -cristobalite” of a diamond structure with an O atom sitting halfway between two Si atoms), but later was cast in doubt due to unrealistically large $\langle \text{Si-O-Si} \rangle$ bond angles ($\sim 180^\circ$) and exceptionally short Si-O bond lengths ($\sim 1.54 \text{ \AA}$) compared with other silica polymorphs ($\sim 146^\circ$ and 1.61 \AA , respectively)^{8,9}. Two popular models were proposed to reconcile this discrepancy: one is the static disorder model which states that high temperature β -cristobalite is composed of static domains of lower-symmetry phases by orientational disorder^{1,9-13}; the other is the dynamic disorder model which argues that β -cristobalite is a disordered structure created by the dynamic superposition of all rigid-unit-modes (RUMs)^{14,15}. Recently, more theoretical calculations^{13,16} were carried out aiming to solve the controversy between these two models, but none of them has given a conclusive answer yet.

Herein we combined classical molecular dynamics (MD) simulations and first-principles calculations at the density functional theory (DFT) level to study the α - β transformation in cristobalite silica and to clarify the disorder nature of high temperature β -cristobalite.

Importantly, we identified the specific local structures constituting the dynamic disorder in β -cristobalite and explored their spatial and temporal correlations. Our study shows: a) a new phase with $I\bar{4}2d$ space group (β' -cristobalite) can be obtained by an isotropic stretching of α -cristobalite in both MD simulations and DFT calculations; b) high temperature β -cristobalite can be obtained through thermally induced α - β or β' - β transformations; c) β -cristobalite is composed of randomly distributed low-symmetry alpha-rings and high-symmetry beta-rings, constantly changing the ring conformation from one to the other; d) autocorrelation time of the ring conformation is on the order of tens of femtoseconds and no spatial correlation is observed, which provide solid evidence for the dynamic disorder in β -cristobalite.

II. DETAILS OF SIMULATIONS

A. Molecular dynamics simulations

For our MD simulations, we used a charge transfer three-body potential¹⁷ that can describe very well both crystalline and amorphous silica (α - and β -cristobalite, α - and β -quartz, high pressure X-I phase, stishovite, phase transformations between α - and β -cristobalite, α - and β -quartz, negative thermal expansion in β -cristobalite and β -quartz, as well as thermomechanical anomalies in silica glass)¹⁷⁻²¹. Essentials for the success of such a potential are that it realistically accounts for the charge redistribution associated with changes in bonding structure and the directional character of the covalent bonding is modeled by angular constraints in terms of three-body interactions. It should be noted that although the force-field used here is quite unique, the key for the discovery of the new β' -cristobalite phase and the subsequent characterization of the

dynamic disorder in β -cristobalite is to explore the negative hydrostatic pressure regime that is largely unexplored experimentally or theoretically.

During all MD simulations in this paper, Nose-Hoover thermostat^{22,23} and Parrinello-Rahman barostat²⁴ were applied when necessary. The long-range Columbic interaction was dealt using the standard Ewald summation technique²⁵ with α/L of 5, where L is the length of the shortest simulation box side, and by using all q vectors with $|q| < 7 \times 2\pi/L$. The real space cutoff was set to be 1.3 nm. We started from a tetragonal unit cell with 4 SiO₂ according to ideal coordinates of α -cristobalite in the *International tables for Crystallography*²⁶ and created a 2592 atom system by duplicating initial unit cell along each axis. We also studied a system of eight times of the original size and found that a system of 2592 atoms is large enough to avoid the system size effect. The 5th order Gear predictor-corrector integration algorithm²⁷ using a time step of 2 fs was adopted throughout all simulations. α - and β -cristobalite were heated up from 300 K to 3000 K under a heating rate of 2.5 K/ps in MD simulations. Statistics of thermodynamic properties were collected for 10 ps after 10 ps equilibration run every 50 K.

B. First-principles calculations

Ab-initio calculations were carried out within the density functional theory (DFT) formalism and the generalized-gradient approximation (GGA), using the Perdew-Burke-Ernzerhof functional²⁸ for the exchange-correlation energy. The calculations were carried out with the SIESTA program²⁹ using a linear combination of atomic orbitals as the basis set, and norm-conserving Troullier-Martins pseudopotentials³⁰. An optimized split-valence double- ζ plus polarized basis set was employed. A real space grid was equivalent to a plane wave cutoff energy of 120 Ry. Γ -point sampling for the super cell's Brillouin zone integration was used,

which is reasonable for a cell with 96 atoms. For each applied pressure, the lattice vectors were optimized together with the atomic coordinates by using the Parrinello-Rahman barostat²⁴.

DFT calculations were carried out here to corroborate MD results in terms of the pressure-induced phase transformation and the small energy difference between α - and β' -cristobalite.

III. RESULTS AND DISCUSSION

A. Structure and stability of β' -cristobalite

Upon an isotropic stretching of α -cristobalite in MD simulations at 300 K up to -2 GPa at 0.1 GPa interval with a rate of 5 MPa/ps, a discontinuity in the density as a function of pressure curve in Fig. 1 clearly indicates a first order transition at -0.6 GPa. The new phase is retained at ambient conditions after releasing pressure to 0 GPa at 300 K. Its space group is identified to be $I\bar{4}2d$ by KPLOT (a program for identifying the space group of a crystal and visualizing the structure)³¹, consistent with a hypothetical structure proposed by Wright and Leadbetter⁹ and also used by O’Keeffe and Hyde¹ as domains to explain the disorder in high temperature β -cristobalite. We tentatively called this new phase β' -cristobalite, to differentiate it from the high temperature β -cristobalite.

In our DFT study, a similar stretching of α -cristobalite was performed as in our MD simulations at 0 K. Figure 1 shows that β' -cristobalite emerges when α -cristobalite is isotropically stretched beyond -1.2 GPa in DFT calculations, confirming that this low-density β' -cristobalite is not an artifact of the potential used in our MD simulations. It can be also seen that when temperature is dropped from 300 to 0 K in MD simulations, the transformation pressure changed from -0.6 to -1.2 GPa, close to the pressure at which the phase transformation takes

place in DFT calculations at 0 K. As shown in Fig. 1, the density in DFT calculations is always lower than that in MD simulations, which is due to the fact that GGA tends to underbind and overestimate lattice constants²⁸.

To our best knowledge, this was the first time that $\bar{I}42d$ silica phase was ever observed in MD simulations or first principles calculations without any restriction on the symmetry of the starting and ending phase, indicating a possible pressure-induced phase transformation pathway between α - and β' -cristobalite. The predicted structure of β' -cristobalite at 300 K ($a = 4.9275 \text{ \AA}$, $c = 7.2677 \text{ \AA}$, $O(x) = 0.0833$) agrees very well with that in other theoretical studies^{16,32} and with the hypothetical structure proposed by Wright and Leadbetter⁹ ($a = 5.042 \text{ \AA}$, $c = 7.131 \text{ \AA}$, $O(x) = 0.079$). It is worth noting that in Refs. 16 and 24, the initial symmetry is pre-fixed to be $\bar{I}42d$, while in our study this structure emerges spontaneously from α -cristobalite upon isotropic stretching without any symmetry constraint.

In order to compare the relative stability of α -, β' - and ideal β -cristobalite, we carried out DFT total energy calculations at different cell volumes without symmetry constraints, following similar procedures in an early work³³. Figure 2 shows that α -cristobalite is stable below $45 \text{ \AA}^3/\text{SiO}_2$, while β' -cristobalite is stable between 45 and $53 \text{ \AA}^3/\text{SiO}_2$. When α -cristobalite is stretched beyond $47 \text{ \AA}^3/\text{SiO}_2$, its energy decreases and gradually overlaps with that of β' -cristobalite instead of increasing following the dashed parabolic line (if with symmetry constraints). This is another indication that β' -cristobalite would naturally emerge when α -cristobalite is expanded beyond certain specific volume. Figure 2 also shows α -, β' - and β -cristobalite are energetically equivalent when the volume is exceeding $53 \text{ \AA}^3/\text{SiO}_2$. A very small energy difference ($\sim 0.01 \text{ eV}/\text{SiO}_2$) between α - and β' -cristobalite was found in our DFT

calculations, in good agreement with other first principles calculations^{10,16,32}. The small energy difference between these two phases allows for the existence of dynamic disorder at high temperature observed in our MD simulations as discussed below.

B. Structure of high temperature β -cristobalite

High temperature β -cristobalite can be obtained by going through either α - β or β' - β transformation between 700 K and 900 K. The high heating rates and the absence of defects and grain boundaries in our simulations are in part responsible for overshooting the α - β transformation temperature of 540 K in experiments. By taking the simulation box as a supercell, neutron diffraction patterns of α -cristobalite and β' -cristobalite at 300 K, β -cristobalite at 1000 K from our MD simulations are calculated and shown in Fig. 3(a). The diffraction pattern of ideal β -cristobalite based on the unit cell with $Fd\bar{3}m$ symmetry is also included for comparison. The diffraction pattern of β -cristobalite at 1000 K from our MD simulations is very different from that of α -cristobalite and β' -cristobalite at 300 K, indicating a distinct phase emerging after α - β and β' - β transformations. Overall the diffraction pattern of β -cristobalite looks very similar to that of ideal β -cristobalite initially proposed by Wyckoff⁷. In terms of the number of peaks and the relative peak intensities, the diffraction pattern of our β -cristobalite at 1000 K is in excellent agreement with the top pattern, which was obtained from neutron total scattering measurements at a spallation source³⁴.

By using 50 frames of atomic configurations generated in MD over 10 ps, we calculated the three-dimensional diffuse scattering based on the structural factor for electron diffraction $S(Q)=\sum f_i \exp(-iQ \cdot r_i)$, where f_i and r_i is the atomic scattering factor and the instantaneous position

of atom i in the unit cell or supercell, respectively, Q takes values in the reciprocal space on a grid given by the size of the simulation box. The three-dimensional diffuse scattering gives more information about the structure of high temperature β -cristobalite than the one-dimensional powder diffraction data. As seen in Fig. 3(b) (the center spot in calculated diffraction patterns is omitted for clarity), the diffuse scattering of β -cristobalite at 1000 K from our MD simulations has similar line features as the diffuse background measured in transmission electron microscopy (TEM)³⁵. While in α -cristobalite at 300 K and in ideal β -cristobalite, such diffuse background is not obvious. The diffuse background in β -cristobalite is attributed to low-energy modes of concerted rotation of tetrahedra activated in the high temperature phase, with the direction of the strong correlation normal to the diffuse planes of intensity^{34,35}. It should be pointed out that $\{400\}$ spots in our calculated TEM pattern of β -cristobalite are much weaker than those from experiments. This may be because our calculations are based on the kinematic theory that does not take into account the multiple scattering effects (e.g, 220 followed by $2\bar{2}0$).

C. Ring conformation changes in high temperature β -cristobalite

The above results show that our silica model can correctly represent the structure and dynamics of high temperature β -cristobalite, which paves the way for a better understanding of the α - β transformation mechanisms and the disorder nature of the high temperature β -phase. To this end, a criterion to differentiate the symmetry of six-membered rings (identified using the shortest-path analysis³⁶) in these phases was constructed. The idea is to track the variance (e.g., the maximum minus the minimum value) of the third nearest neighbor O-O distance in six-membered rings shown in Fig. 4(a). High-symmetry rings like beta-rings in β -cristobalite (3 fold rotation around $[01\bar{1}]$) generally have a smaller O-O variance (peak around 0.1 Å, see Fig. 4(b)),

while low-symmetry rings like alpha-rings in α -cristobalite (2 fold rotation around $[01\bar{1}]$) have a larger O-O variance (peak around 1.9 Å, see Fig. 4(b)). So we choose the O-O variance of 1.0 Å as a suitable value to differentiate the high-symmetry beta-rings from the low-symmetry alpha-rings.

Using this method, we quantified the relative proportion of alpha-rings versus beta-rings throughout α - β and β' - β transformations (the latter transformation occurs at a slightly lower temperature). Figure 5(a) shows that the alpha-ring fraction relaxes to ~ 0.42 after 850 K in both routes and then gradually increases with temperature and saturates after 2500 K. The fact that the alpha-ring fraction never approaches either zero or one after the transformation temperature provides solid evidence that high temperature β -cristobalite cannot be just an orientational disorder of single phase domains proposed by either Wright and Leadbetter⁹ or Hatch and Ghose¹².

D. Temporal correlation of ring conformations

To better understand the structure of high temperature β -cristobalite, a temporal correlation of the ring conformation was examined. Basically, at each temperature, we tracked the conformation of each ring over time and correlated with its status at the time origin. Each ring was assigned the status value of 1 at the time origin, if it changed from one conformation to another, its status value changed to 0. The conformation evolution of all the alpha-rings and beta-rings in the system is averaged to give the corresponding autocorrelation, respectively. Above the transformation temperature, autocorrelations of the alpha-ring status in Fig. 5 (b) inset show a quick de-correlation (a similar behavior is observed for beta-rings) and the characteristic time is on the order of 20-50 fs, in contrast with 1 ps relaxation time predicted in the static

disorder model⁹. The quick de-correlation of the ring status rules out the possibility of static domains and directly supports the dynamic nature of the disorder in high temperature β -cristobalite. By fitting an exponential function to the autocorrelation curve, we estimated the conversion rate (k) between alpha- and beta-rings. Arrhenius plots of the alpha-beta and beta-alpha ring conversion rates are shown in Fig. 5(b), from the slopes of the two fitted straight lines we calculated the enthalpy for the alpha-to-beta and beta-to-alpha ring conversion to be 13.81 and 31.79 meV/SiO₂, respectively. This gave an enthalpy difference of 17.98 meV/SiO₂ between alpha- and beta-ring, if we assume the alpha-to-beta and beta-to-alpha ring conversion go through the same transition state. The enthalpy difference between these two conversion processes indicates that the beta-to-alpha ring conversion has stronger temperature dependence than the alpha-to-beta ring conversion. With increasing temperature, more beta-rings convert into alpha-rings than alpha-rings convert into beta-rings, so the population of alpha-rings increases with temperature as seen in Fig. 5(a). This explains the nearly zero or even negative thermal expansion in high temperature β -cristobalite³⁷ (inset of Fig. 5(a) shows the density as a function of temperature from our MD simulations), as α -cristobalite has a higher density than β -cristobalite²⁰. Such conformational changes are remnant in silica and silica-rich glasses, which explain the most pronounced elastic anomalies in these systems¹⁹, e.g., the positive temperature derivative^{38,39} and the negative pressure derivative of elastic moduli^{40,41}.

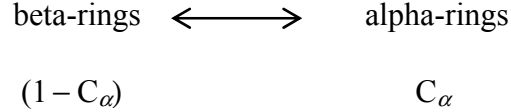
E. Spatial correlation of ring conformations

To check the possibility of co-existence of multiple phase domains in β -cristobalite, radial distribution functions (RDF) of six-membered ring centers ($\vec{r}^c = \frac{1}{12} \sum_{i=1}^{12} \vec{r}_i$, including six Si and six

O atoms) were calculated to study the spatial correlation of the ring conformation. If we consider each ring as a united atom, the ring center RDF can be simply understood as a particle-particle pair distribution function. At 300 K, the alpha-alpha ring center RDF in α -cristobalite and the beta-beta ring center RDF in β -cristobalite look very similar to each other (Fig. 6 (a)). Fewer peaks in the ring center RDF in β -cristobalite can be attributed to a higher symmetry of this structure. Above the transformation temperature, three pair correlations (alpha-alpha, beta-beta and alpha-beta) overlap almost perfectly with each other at all temperatures (900 K and 3000 K are shown in Fig. 6(b)-(c)), except some thermal broadening effect in the peak intensity. This suggested a total random (species-blind) distribution of alpha- and beta-rings on a $P4_12_12$ lattice (like random substitutional solid solution with alpha- and beta-rings acting like A and B type of atoms) in the high temperature β -cristobalite. As if alpha- or beta-rings have any preference in occupying neighboring lattice sites, their ring center RDFs would not be identical.

F. Dynamics in high temperature β -cristobalite

Figure 5(b) and 6(b)-(c) provide us a clear picture of the dynamic disorder in high temperature β -cristobalite: a) flipping from alpha- to beta-rings and beta- to alpha-rings are purely thermal activated processes with fixed rates at a specific temperature; b) no spatial correlations exist between any six-membered rings. These build a solid foundation for us to have a much better understanding of the alpha-ring proportion as a function of temperature data in Fig. 5(a), which shows its fraction after α - β and β' - β transformations has a very small fluctuation at each temperature (less than 1%). Hence the conversion between beta-rings and alpha-rings at a specific temperature above the transformations can be understood as the following “chemical equilibrium”:



where C_α and $(1 - C_\alpha)$ is the equilibrium population of alpha-rings and beta-rings at a specific temperature above the phase transformations. From this we can derive a relationship between the activation free energy difference $\Delta G = G_\alpha - G_\beta = \Delta G_{\beta \rightarrow \alpha} - \Delta G_{\alpha \rightarrow \beta}$ (see Fig. 7), and the alpha-ring fraction C_α :

$$\ln\left[\frac{C_\alpha}{(1 - C_\alpha)}\right] = -\frac{\Delta G}{kT} = -\frac{\Delta H}{kT} + \frac{\Delta S}{k} \quad (1)$$

where k is the Boltzmann constant, T is the absolute temperature, ΔG , ΔH and ΔS is the Gibbs free energy, enthalpy and entropy change associated with the beta- to alpha-ring conversion, respectively. By fitting eq. (1) to the alpha-ring fraction versus temperature data from 950 to 3000 K in Fig. 5(a), as shown in Fig. 5(c), the enthalpy change (ΔH) is estimated from the slope to be 18.6 meV/SiO₂, in a reasonable agreement with the value of 12 meV/SiO₂ in DFT calculations at 0 K¹⁶, comparable to the value obtained from the above conversion rate analysis (17.98 meV/SiO₂). Therefore we can consider the conversion between beta-rings and alpha-rings as a first order forward and backward “reaction” (conversion), the rates can be estimated from the autocorrelations of the ring status shown in Fig. 5 (b) at a specific temperature above the transformations.

From the above chemical equilibrium analysis in Fig. 5(c), the entropy change (ΔS) is estimated from the fitted line intercept with y axis to be 0.01546 meV·K⁻¹/SiO₂. Right after the transformation, for example at 950 K, $\Delta G = 3.91$ meV/ SiO₂, which means $G_\alpha > G_\beta$, beta-rings are more stable than alpha-rings. At higher temperatures, for example at 2000 K, $\Delta G = -12.32$ meV/ SiO₂, which means $G_\alpha < G_\beta$, alpha-rings become more stable than beta-rings. So the positive

entropy change associated with the beta-ring to alpha-ring conversion is the key to understanding why the alpha-ring fraction increases with temperature in Fig. 5 (a).

From the above detailed structural analysis, it becomes clear that the thermally induced α - β transformation in cristobalite silica can be understood as an order-disorder transition, in which the basis units (alpha- or beta-rings) can be randomly distributed on a $P4_12_12$ lattice at high temperatures but with a long range order below α - β and β - β transformations. In this sense, the α - β phase transformation is equivalent to a spin magnetic transition on the same lattice. In this case, rings (similar to spins) can be in one of two states (alpha- or beta-rings) in β -cristobalite. Our simulations show that, above the transformation temperature, there is no spatial correlation of the ring conformation beyond the unit cell length scale; it would not be meaningful to discuss the existence of any domains, either static or dynamic in nature in β -cristobalite. The conformational disorder in β -cristobalite gives the underlying topology framework the flexibility to undergo facile low-energy distortions via, e.g. the rigid unit modes (RUMs)^{14,15}.

IV. CONCLUSIONS

Our study, for the first time clearly identified the local structures constituting the dynamic disorder in β -cristobalite, and quantified it in terms of the temporal and spatial correlations of ring conformations and the energetics for the inter-conversions between them. These insights provide important clues on how to characterize the true local structures of β -cristobalite in experiments, which has confounded scientists for decades. Moreover, our study indicates that to stabilize β -cristobalite-related structures as engineering ceramics with high thermal shock resistance, it is of critical importance to preserve the conformational disorder, not the apparent

crystal symmetry. It is the conformational disorder that is accounted for the nearly zero or even negative thermal expansion in β -cristobalite, resulting in the high thermal shock resistance.

ACKNOWLEDGMENTS

This work is supported by the National Science Foundation under Grant No. DMR-907076. We thank Drs. J. Kieffer, M. Durandurdu and Y. F. Shi for their stimulating discussions.

Figure Captions

FIG. 1. Density as a function of pressure during the pressure-induced α - β' transition in cristobalite silica from MD simulations at 300 K, 0 K and from DFT at 0 K.

FIG. 2. Total energy versus volume curves for α -, β' - and ideal β -cristobalite from DFT calculations without symmetry constraints.

FIG. 3. Comparison between experimental and calculated diffraction patterns of cristobalite silica. (a) Neutron diffraction pattern of α - and β' -cristobalite at 300 K, β -cristobalite at 1000 K from our MD simulations and ideal β -cristobalite with symmetry of $Fd\bar{3}m$, the diffraction pattern of β -cristobalite at 950 K from neutron total scattering measurements is shown at the top for comparison³⁴. (b) Calculated diffuse scattering of α -cristobalite at 300 K, β -cristobalite at 1000 K using atomic configurations generated in MD and ideal β -cristobalite. The electron diffraction

pattern of β -cristobalite at 620 K from TEM measurement³⁵ is included for comparison. Note: all diffraction patterns in (b) are for the [001] zone axis.

FIG. 4. Alpha- and beta-ring differentiation. (a) Crystal structure of α -, β - and ideal cristobalite and the corresponding ring in each phase. Both alpha- and beta-rings ring are viewed from the $[01\bar{1}]$ direction and the pink line indicates the (111) plane. (b) Relative probability distribution of the O-O variance in alpha-rings (peak around 1.9 Å) and beta-rings (peak around 0.1 Å) at 300 K, black vertical ticks are the corresponding ones at 0 K.

FIG. 5. Alpha- and beta-ring conversions with increasing temperature. (a) Alpha ring fraction as a function of temperature for α - β and β - β transformation, the inset shows the corresponding density change as a function of temperature. (b) Arrhenius plots of the alpha-beta and beta-alpha ring conversion rates (k) above the α - β transformation, the inset shows the autocorrelation of the alpha-ring status versus time at 1200 K, 1800 K, 2400 K and 3000 K. (c) $\ln\left[\frac{C_\alpha}{(1-C_\alpha)}\right]$ versus $1/T$, where C_α is the alpha-ring fraction from 950 to 3000 K in (a).

FIG. 6. Ring center radial distribution function (RDF) at 300 K for α - and β -cristobalite (a), at 900 K for β -cristobalite (b) and at 3000 K for β -cristobalite (c).

FIG. 7. A schematic diagram of the energy barriers for alpha-ring to beta-ring and beta-ring to alpha-ring conversion.

Figures

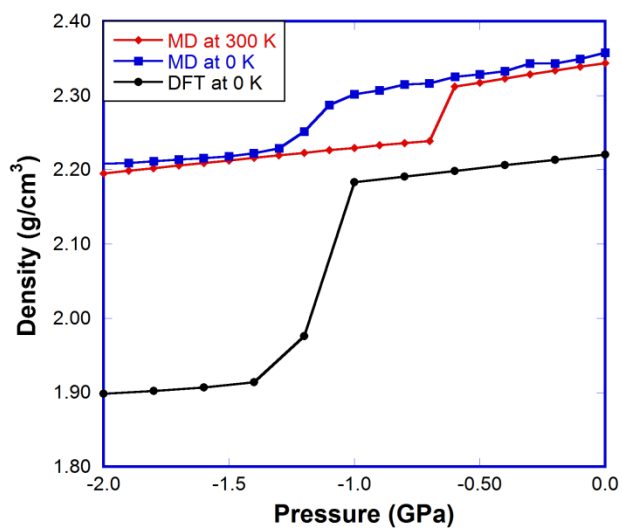


Fig. 1. Yuan and Huang, 2012

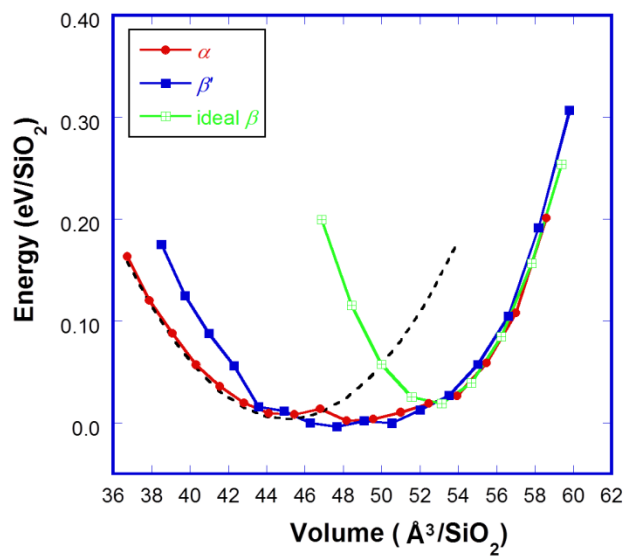


Fig. 2. Yuan and Huang, 2012

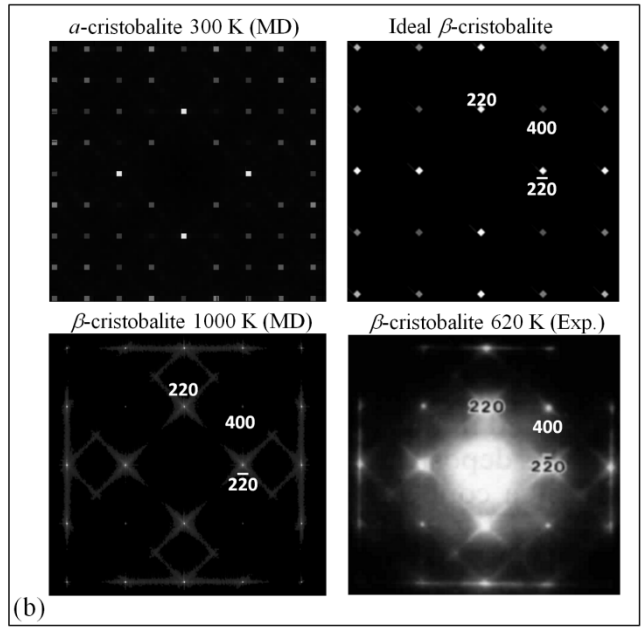
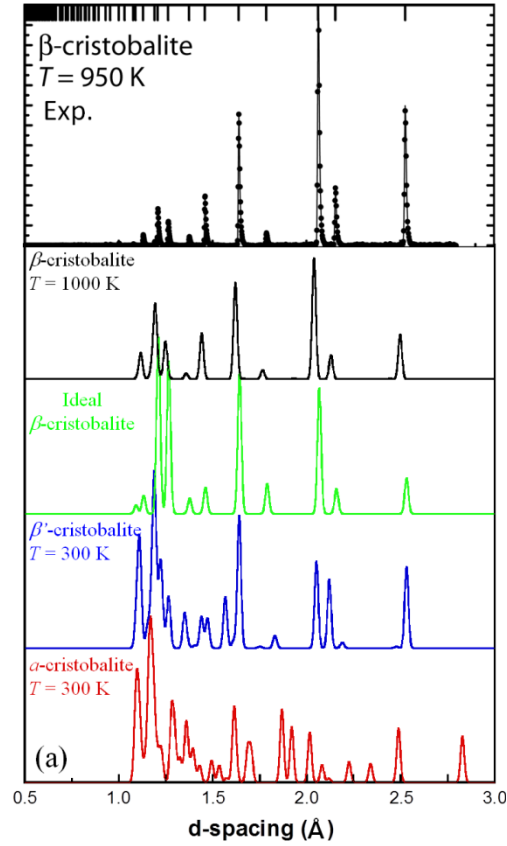


Fig. 3. Yuan and Huang, 2012

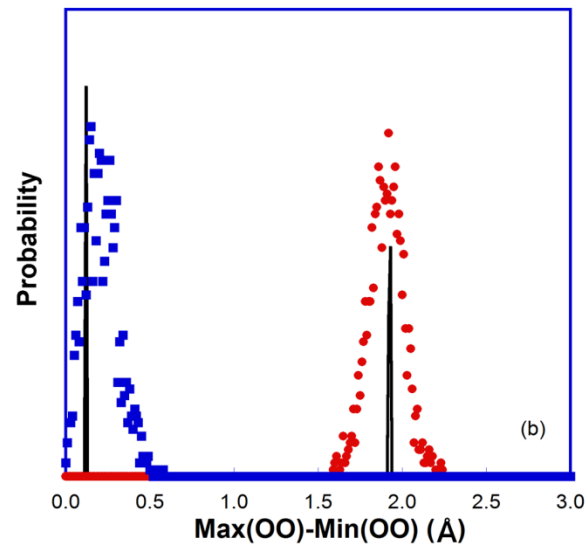
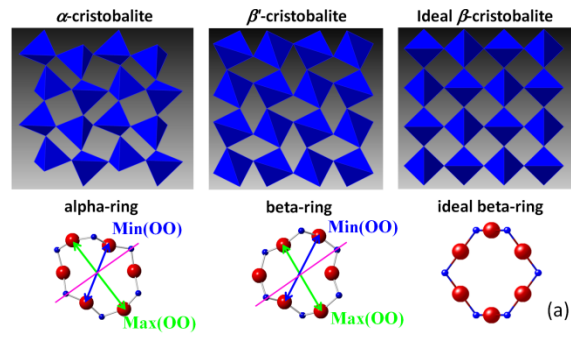


Fig. 4. Yuan and Huang, 2012

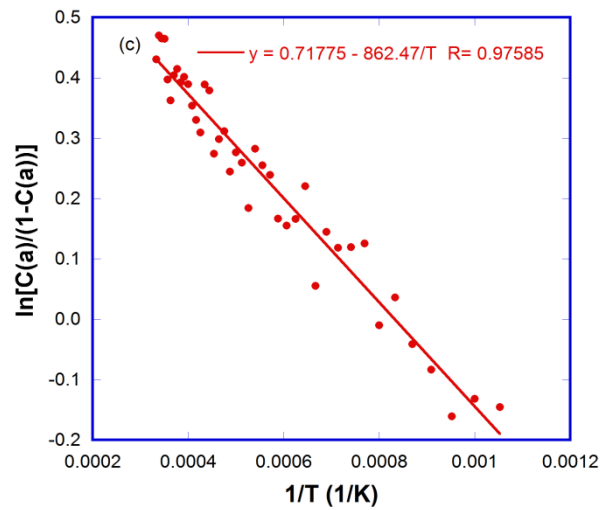
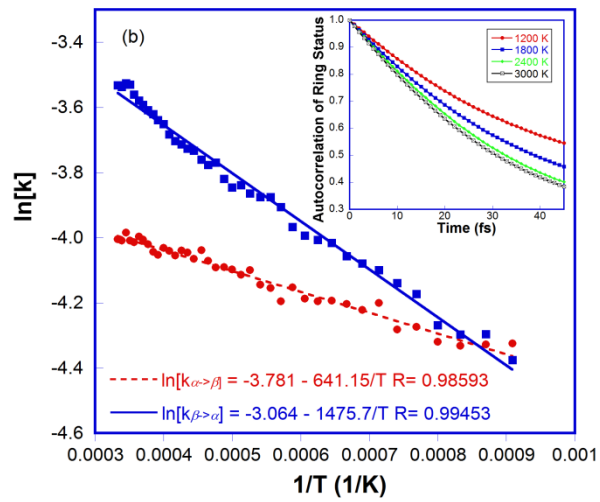
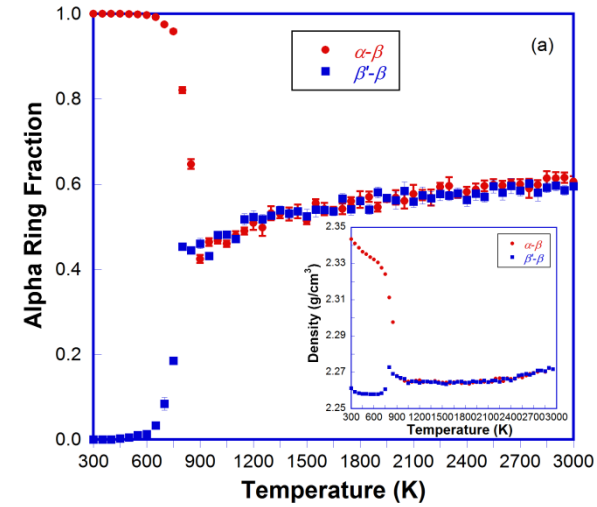


Fig. 5. Yuan and Huang, 2012

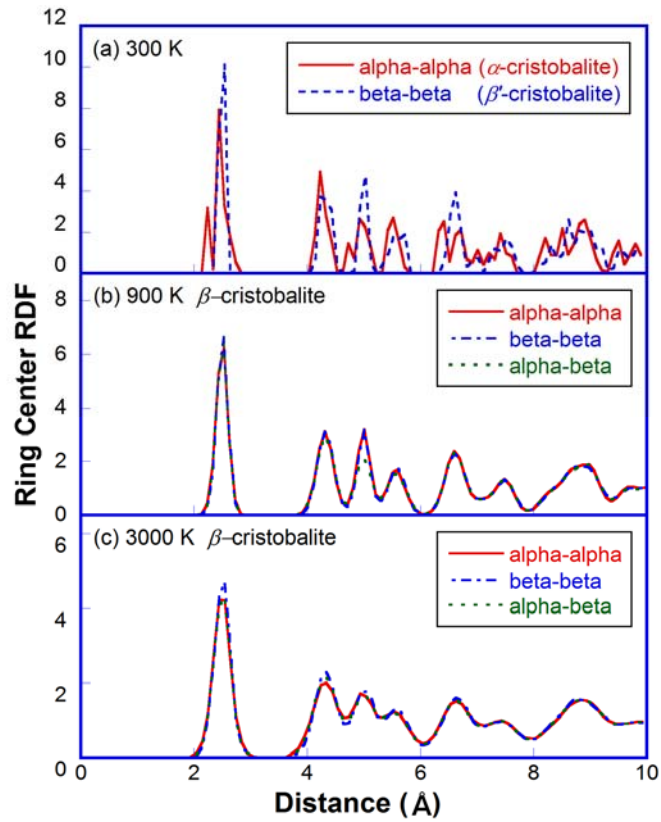


Fig. 6. Yuan and Huang, 2012

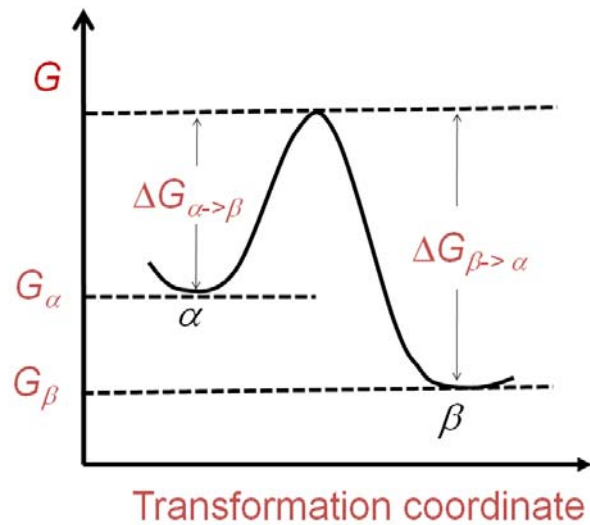


Fig. 7. Yuan and Huang, 2012

- ¹ M. O’Keeffe and B. Hyde, *Acta Crystallogr., Sect. B: Struct. Sci.* **32**, 2923-2936 (1976).
- ² J.G. Thompson, R.L. Withers, S.R. Palethorpe, and A. Melnitchenko, *J. Solid State Chem.* **141**, 29-49 (1998).
- ³ A. Perrotta, D. Grubbs, E. Martin, N. Dando, H. Mckinstry, and C. Huang, *J. Am. Ceram. Soc.* **72**, 441-447 (1989).
- ⁴ E.S. Thomas, J.G. Thompson, R.L. Withers, M. Sterns, Y. Xiao, and R.J. Kirkpatrick, *J. Am. Ceram. Soc.* **77**, 49-56 (1994).
- ⁵ M. Weldon, K. Queeney, J. Eng, K. Raghavachari, and Y. Chabal, *Surf. Sci.* **500**, 859-878 (2002).
- ⁶ D.A. Keen and M.T. Dove, *Mineral Mag* **64**, 447-457 (2000).
- ⁷ R.W.G. Wyckoff, *Am. J. Sci.* **s5-9**, 448-459 (1925).
- ⁸ D. Peacor, *Z. Kristallogr.* **138**, 274-298 (1973).
- ⁹ A. Wright and A. Leadbetter, *Philos. Mag.* **31**, 1391-1401 (1975).
- ¹⁰ F. Liu, S.H. Garofalini, R.D. King-Smith, and D. Vanderbilt, *Phys. Rev. Lett.* **70**, 2750-2753 (1993).
- ¹¹ M. Zhang and J.F. Scott, *J. Phys.: Condens. Matter* **19**, 275201 (2007).
- ¹² D. Hatch and S. Ghose, *Phys. Chem. Miner.* **17**, 554-562 (1991).
- ¹³ E. Cope and M. Dove, *J. Phys.: Condens. Matter* **22**, 125401 (2010).
- ¹⁴ I.P. Swainson and M.T. Dove, *Phys. Rev. Lett.* **71**, 193-196 (1993).
- ¹⁵ I.P. Swainson and M.T. Dove, *Phys. Rev. Lett.* **71**, 3610-3610 (1993).
- ¹⁶ S. Coh and D. Vanderbilt, *Phys. Rev. B* **78**, 054117 (2008).
- ¹⁷ L. Huang and J. Kieffer, *J. Chem. Phys.* **118**, 1487-1498 (2003).

- ¹⁸ L. Huang and J. Kieffer, Phys. Rev. B **69**, 224204 (2004).
- ¹⁹ L. Huang and J. Kieffer, Phys. Rev. B **69**, 224203 (2004).
- ²⁰ L. Huang and J. Kieffer, Phys. Rev. Lett. **95**, 215901 (2005).
- ²¹ L. Huang and J. Kieffer, Appl. Phys. Lett. **89**, 141915 (2006).
- ²² S. Nose, Mol. Phys. **52**, 255-268 (1984).
- ²³ S. Nose, J. Chem. Phys. **81**, 511-519 (1984).
- ²⁴ M. Parrinello and A. Rahman, Phys. Rev. Lett. **45**, 1196-1199 (1980).
- ²⁵ P.P. Ewald, Ann. Phys. **369**, 253-287 (1921).
- ²⁶ T. Hahn, *International tables for crystallography. Brief teaching edition of volume A, space-group symmetry* (Published for the International Union of Crystallography by D. Reidel Pub. Co., 1985).
- ²⁷ C.W. Gear, *Numerical Initial Value Problems in Ordinary Differential Equations* (Prentice Hall PTR, Upper Saddle River, NJ, USA, 1971).
- ²⁸ J. Perdew, K. Burke, and M. Ernzerhof, Phys. Rev. Lett. **77**, 3865-3868 (1996).
- ²⁹ P. Ordejon, E. Artacho, and J. Soler, Phys. Rev. B **53**, 10441-10444 (1996).
- ³⁰ N. Troullier and J. Martins, Phys. Rev. B **43**, 1993-2006 (1991).
- ³¹ R. Hundt, J. Schon, A. Hannemann, and M. Jansen, J. Appl. Crystallogr. **32**, 413-416 (1999).
- ³² T. Demuth, Y. Jeanvoine, J. Hafner, and J. Angyan, J. Phys.: Condens. Matter **11**, 3833-3874 (1999).
- ³³ L. Huang, M. Durandurdu, and J. Kieffer, Nat. Mater. **5**, 977-981 (2006).
- ³⁴ M.G. Tucker, M.P. Squires, M.T. Dove, and D.A. Keen, J. Phys.: Condens. Matter **13**, 403-423 (2001).
- ³⁵ G. Hua, T. Welberry, R. Withers, and J. Thompson, J. Appl. Crystallogr. **21**, 458-465 (1988).

- ³⁶ C. Mariani and L. Hobbs, *J. Non-Cryst. Solids* **106**, 309-312 (1988).
- ³⁷ E. Bourova and P. Richet, *Geophys. Res. Lett.* **25**, 2333-2336 (1998).
- ³⁸ R. Youngman, J. Kieffer, J. Bass, and L. Duffrene, *J. Non-Cryst. Solids* **222**, 190-198 (1997).
- ³⁹ A. Polian, D. Vo-Thanh, and P. Richet, *EuroPhys. Lett.* **57**, 375-381 (2002).
- ⁴⁰ M. Grimsditch, *Phys. Rev. Lett.* **52**, 2379-2381 (1984).
- ⁴¹ C. Zha, R. Hemley, H. Mao, T. Duffy, and C. Meade, *Phys. Rev. B* **50**, 13105-13112 (1994).